TECHNICAL PAPER

fib WILEY

Strengthening of reinforced concrete beams in shear using different steel reinforced grout techniques

Tadesse G. Wakjira[1] | Usama Ebead[2]

[1]Department of Civil and Architectural Engineering, Qatar University, Doha, Qatar

[2]ASCE member, Professor of Structural Engineering, Department of Civil and Architectural Engineering, Qatar University, Doha, Qatar

Correspondence
Usama Ebead, ASCE member, Professor of Structural Engineering, Department of Civil and Architectural Engineering, Qatar University, P. O. Box 2713, Doha, Qatar.
Email: uebead@qu.edu.qa

Abstract

In this study, steel reinforced grout (SRG) is proposed for shear strengthening of reinforced concrete (RC) beams using the near-surface embedded (NSE) technique. It is believed based on several research contributions in the literature that the NSE technique precludes or delays the onset of premature debonding and achieves higher strength increase in strengthened beams compared to the externally bonded (EB) counterpart. The tests conducted in this study used 13 RC beams to determine the shear behavior of RC beams strengthened in shear using SRG. The effect of the strengthening technique (NSE versus EB), SRG fabric density, strengthening scheme (side-bonded vs. U-wrapped), and the strengthening configuration (continuous vs. discontinuous) on RC shear enhancement was studied. The strengthening effectiveness of the SRG system was assessed in terms of the shear capacity, failure mechanism, load-deflection response, and strain results. The NSE-SRG increased the beam shear strength by an average of 100%, alleviated SRG debonding, and enhanced the deformation characteristics. The average increase in the shear strength of the EB-SRG strengthened beam was 54% and 105% for the continuous and discontinuous SRG strips, respectively. An analytical model is proposed to predict the shear capacity of both the NSE-SRG and EB-SRG strengthened beams and give accurate and safe predictions.

KEYWORDS

concrete, shear strength, steel reinforced grout, strengthening

1 | INTRODUCTION

Strengthening of civil infrastructures is usually necessary to address deficiencies caused by various factors such as a change in the use of a structure, material degradation, lack of proper maintenance, corrosion of reinforcement bars, and earthquake-induced damage. The increasing demand to upgrade civil infrastructure has resulted in advanced systems for innovative strengthening and rehabilitation particularly in the use of composites.[1,2] Such strengthening systems include fiber reinforced polymer (FRP) applied using either the externally bonded (EB) technique[3–8] or the near-surface mounted[9–13] technique, the EB fabric reinforced cementitious matrix (FRCM),[2,14–18] the near-surface embedded (NSE)

FRCM,[19] and the hybrid NSE/EB-FRCM.[20,21] These composites are usually comprised of carbon, basalt, glass, and/or polyparaphenylene benzobisoxazole (PBO) fibers embedded within organic matrices (generally epoxy resin) in FRP and fabrics embedded within the cementitious matrix in FRCM.

Recently, composites that utilize high strength steel fabrics have been proposed as cost-effective and promising alternative strengthening solutions.[22–28] Steel fabrics comprise unidirectional ultra-high tensile strength (UHTS) galvanized steel micro-cords. Such materials can be applied to structural members through the wet lay-up method using either polymeric resin in steel reinforced polymer (SRP) or inorganic matrix in steel reinforced grout (SRG). The first studies on the potential strengthening application of SRG/SRP for structural members dated back in 2005.[24,29] Previous experimental studies have demonstrated the successful application of SRG/SRP for strengthening RC beams,[30–33] RC columns confinement,[34–36] and masonry structures.[25,26,37] The field strengthening application of SRP for under-reinforced concrete bridge has also been studied.[38] The use of inorganic matrix in SRG instead of epoxy adhesives in SRP offers advantages such as compatibility with the substrate (e.g., masonry, concrete), ease of application on a wet surface or at low temperature, improved fire resistance, and a further reduction in cost.[39]

The results of previous experimental studies[24,30–33,40] have demonstrated the effectiveness of SRG for strengthening of RC beams in flexure. Nonetheless, research on the application of this technique for strengthening shear deficient beams is scarce.[41–43] In addition, previous studies focused on the use of an SRG system for EB strengthening. The failure of EB-SRG strengthened beams, similar to that of EB-FRCM, is mostly attributed to SRG debonding.[24,30–32,40,41,43] This type of failure limits the strength of the composite. In contrast, recent studies have demonstrated that the use of the NSE and the hybrid NSE/EB techniques can be an effective approach to improve the concrete/FRCM bond, thereby delaying or precluding the undesired premature debonding observed in the EB technique.[19–21,44] As a result, the use of these techniques yielded better utilization of the FRCM composite.[19–21,44] The NSE technique also provides protection for the strengthening material, unlike the EB technique where the material is exposed to weather conditions and is also susceptible to fire and vandalism. This technique provides similar advantages as that of the near surface mounted technique for FRP in which the FRP reinforcement bars or strips are embedded in a narrow slit of grooves made on the concrete cover.[45–47] The NSE-SRG strengthening involves cutting grooves on the concrete surface and installation of the SRG composite in the prepared grooves retaining the original dimension of the beams. Thus, the number of SRG fabric layers that can be installed in the NSE technique is limited to a certain number that can be embedded within the concrete cover.

This study investigated the performance of shear-strengthened RC beams with different SRG techniques to address the aforementioned research gaps. The use of the NSE technique for the SRG system was investigated and its performance was compared with that of the conventional EB technique. Other experimental parameters were investigated, including the fabric density, presence of a U-wrap scheme, and the strengthening amount in a continuous or discontinuous configuration in shear-strengthened RC beams. The experiments revealed the strengthening capability of SRG for shear-critical beams. In addition, a model for determining the shear capacity of RC beams strengthened with an SRG system was proposed and results obtained from the model were compared with experimental results.

2 | TEST PROGRAM

Thirteen full-scale RC beams with identical geometry and internal reinforcement were constructed and tested. Twelve beams were strengthened in shear with different SRG systems applied using either the EB or NSE technique, whereas one beam was used as a reference.

2.1 | Materials

The tested beams were cast from a single concrete batch of ready-mix concrete. Compression standard tests conducted on eight 100 mm × 200 mm concrete cylinders revealed a concrete compressive strength of 34 MPa (SD = 1.57 MPa). D20 (20 mm nominal diameter) and D8 (8 mm nominal diameter) bars were used for the flexural reinforcement and transverse reinforcement outside the critical shear span, respectively. The measured yield strength of the D20 and D8 bars were 584 MPa (SD = 0.176 MPa) and 535 MPa (SD = 0.208 MPa), respectively, whereas the yield strains were 0.269% and 0.258%.

The SRG composite was comprised of steel fiber fabrics made of unidirectional UHTS galvanized steel micro-cords. Two types of steel fabrics different in their densities of 1.57 cords/cm and 3.14 cords/cm were used in the SRG composite, which are designated as low- and high-density fabrics, as shown in Figure 1a,b, respectively. The area of the steel fibers per unit width (t_{sf}) was

0.084 mm and 0.169 mm for the low- and high density fabrics, respectively.[48] The steel fibers had the tensile strength ($f_{t,\ sf}$), elastic modulus (E_{sf}), and ultimate strain ($\varepsilon_{sf,\ u}$) of 3 GPa, 190 GPa, and 2.0%, respectively.[48]
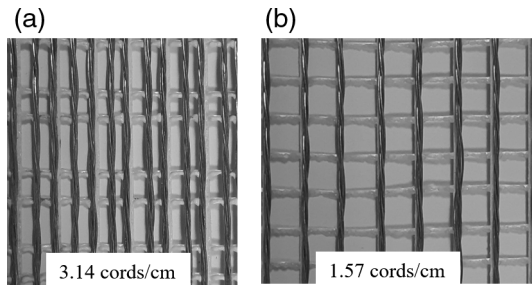
2.2 | Sample details and strengthening

The beams have an overall length of 2,550 mm and a rectangular cross-section of 180 mm × 400 mm (width × depth), as shown in Figure 2a. The flexural reinforcements comprise five D20 bars at the bottom and two D20 bars at the top of the beam (Figure 2a). The internal transverse reinforcement comprises D8 stirrups with 75 mm spacing outside the shear span. The beams were under reinforced in shear; that is, no shear reinforcement was used in the critical shear span of 0.87 m. The beams were strengthened in the critical shear span, as shown in Figure 2b. The beams were designed to study the effect of the following parameters:

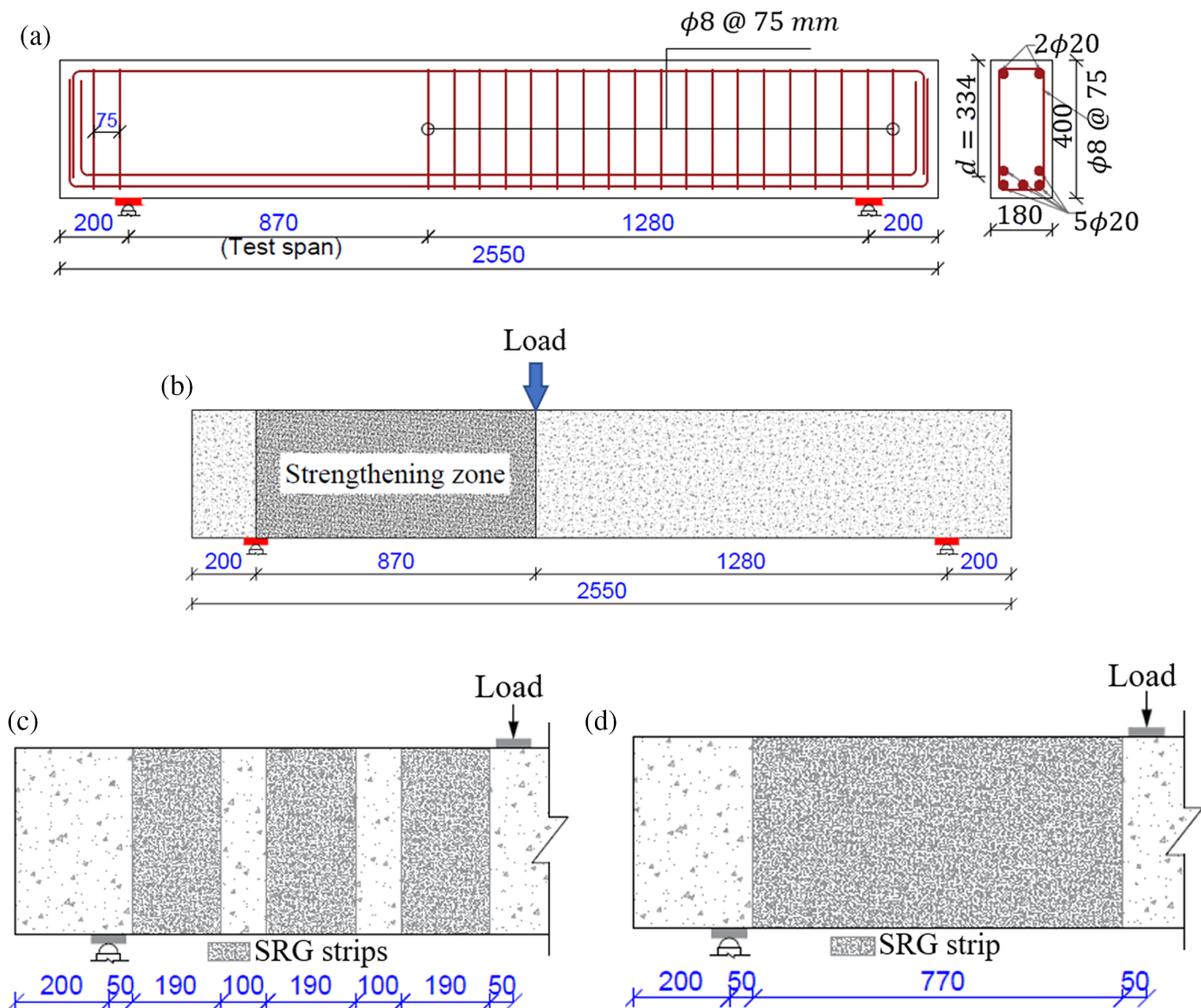(1) Steel fabric density (1.57 cords per centimeter and 3.14 cords per centimeter),

FIGURE 1 The steel fabrics used in this study

FIGURE 2 Details of tested beams (a), strengthening area (b), and SRG layout (c and d) (dimensions in mm). SRG, steel reinforced grout

TABLE 1 Details of the tested beam specimens

Beam ID	Technique	Strengthening scheme	SRG configuration, fabric density	ρ_f (‰)	K_{sf} (MPa)
[a]R	Reference	–	–	–	–
[a]ECUH	EB	U-wrap	C, H	3.756	714
[a]ECUL	EB	U-wrap	C, L	1.867	355
EDUH	EB	U-wrap	D, H	2.461	468
EDUL	EB	U-wrap	D, L	1.223	232
EDSH	EB	Side bonded	D, H	2.461	468
EDSL	EB	Side bonded	D, L	1.223	232
ECSH	EB	Side bonded	C, H	3.756	714
ECSL	EB	Side bonded	C, L	1.867	355
NDUH	NSE	U-wrap	D, H	2.461	468
NDUL	NSE	U-wrap	D, L	1.223	232
NDSH	NSE	Side bonded	D, H	2.461	468
NDSL	NSE	Side bonded	D, L	1.223	232

Note: EB for externally bonded; NSE for near-surface embedded; C for continuous SRG configuration; D for discontinuous SRG configuration; L for low-density fabrics; H for high-density fabrics; ρ_f = SRG geometric reinforcement ratio; K_{sf}= axial rigidity of SRG.
[a]Specimens included in.[43]

(2) Presence of a U-wrap scheme,

(3) SRG strengthening amounts in a continuous SRG strip (Figure 2b) or discontinuous 190 mm wide strips with 100 mm clear spacing (Figure 2c), and.

(4) Type of strengthening technique (EB-SRG versus NSE-SRG for discontinuous configuration).

The test beams and the test parameters are listed in Table 1. The reference beam is labeled R. The strengthened beams are identified using the notation VWXY: V denotes the strengthening technique, where "E" and "N" represent EB-SRG and NSE-SRG, respectively; W denotes the geometric configuration, where "C" and "D" represent continuous and discontinuous configurations, respectively; X denotes the strengthening scheme, where "U" and "S" represent U-jacket and side bonded, respectively; and Y denotes the density of the steel fabrics, where "H" and "L" represent high-, and low-density fabrics, respectively, as presented in Table 1. For instance, ECUH stands for the specimen strengthened with an externally bonded continuous U-jacket of SRG made of high-density steel fabrics.

The strengthening system utilized two layers of unidirectional steel fiber sheets in the SRG composite. In the EB-SRG, the concrete surface was sandblasted and roughened prior to the installation of the SRG, unlike the NSE-SRG that does not require surface preparation owing to the inherited roughened surface due to removing the concrete cover during creating the grooves. Figures 3a–c show the relevant steps related to the application of SRG. The SRG composite in the NSE-SRG system is installed into pre-cut grooves opened on the concrete cover of the lateral faces and/or bottom face of the beam. The strengthening procedure was: (a) the surfaces of the beams were sandblasted and prepared for an EB-SRG strengthened beams; (b) the prepared surface in an EB-SRG and prepared grooves in the NSE-SRG beams are further cleaned and dampened with water; (c) first coat of 4 mm thick geo-mortar is applied on the prepared surface and grooves as per manufacturers' recommendation,[40] as shown in Figure 3a for the NSE-SRG; (d) the steel fabrics are cut as per the desired size, installed and fully impregnated with the matrix; (e) the second coat of 4 mm thick matrix and second fabric layer installed and fully impregnated with the underlying mortar layer, as shown in Figure 3b for NSE-SRG; (f) the final fabric layer is covered with the mortar (4 mm thick) and finished (Figure 3c); (g) the specimens cured for 28-days before testing. Further details of the strengthening procedure can be referred elsewhere for the EB[43] and NSE techniques.[19]

2.3 | Instrumentations

The specimens were tested monotonically in a simply supported three-point displacement-controlled loading configuration at a supporting span of 2.15 m, as shown in Figure 4. As shown in Figure 4, load cell was used to precisely measure the reaction at each support. As shown in Figure 4, the deflection at the loaded beam section was monitored with linear variable displacement transducers. Strain gauges were used to monitor the strains in the

FIGURE 3 Application of the SRG composite for the NSE-SRG. NSE, near-surface embedded; SRG, steel reinforced grout

(a)

(b)

(c)
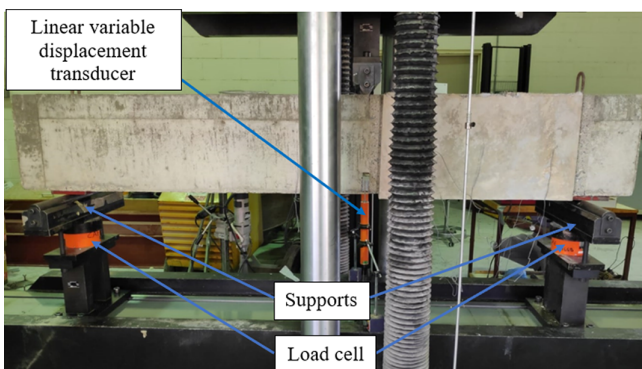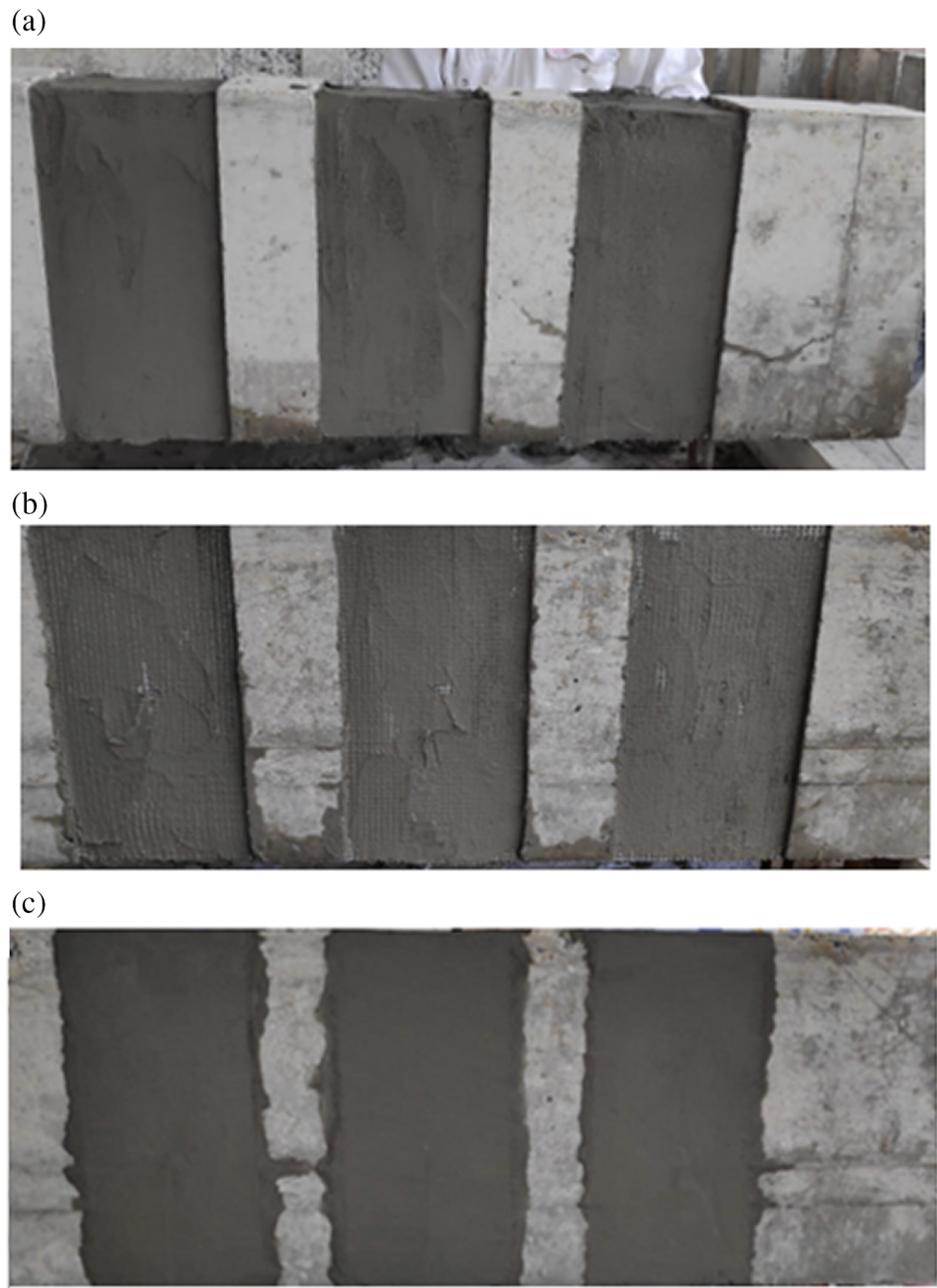
FIGURE 4 Test set-up (dimensions in mm)

Linear variable displacement transducer

Supports

Load cell

flexural reinforcement and concrete strains in the compressive zone.

3 | EXPERIMENTAL RESULTS AND DISCUSSION

Table 2 presents the results of the experiments, including the shear capacity, V_{max}, the beam deflection under the loading point, δ_{max} corresponding to V_{max}, and the percentage increase in δ_{max} compared with the reference beam. Assuming that $\Delta V_{max} = V_{max} - V_{max}^R$, where V_{max}^R and V_{max} are the shear capacities of the reference beam

TABLE 2 Test results

Beam ID	V_{max} (kN)	$\Delta V_{max}/V_{max}^R$ (%)	δ_{max} (mm)	Increase in δ_{max}(%)	ψ (kN.Mm)	$\Delta\psi$ (%)	ε_c (‰)	V_{pr} (kN)	V_{pr}/V_{ex}
R	112	–	3.97	–	375.6	–	0.595	107	0.96
ECUH	261	133	11.4	187	2,813	649	0.574	247	0.95
ECUL	238	112	10.2	156	2,280	507	1.891	210	0.88
EDUH	204	82	8.77	121	1,674	346	1.918	178	0.87
EDUL	171	53	6.23	57	917	144	0.709	159	0.93
EDSH	166	48	6.47	63	948	152	0.964	178	1.07
EDSL	147	32	5.96	50	831	121	0.916	159	1.08
ECSH	226	102	9.41	137	1951	419	1.722	247	1.09
ECSL	192	72	6.91	74	1,118	198	1.077	210	1.09
NDUH	250	124	10.8	171	2,501	566	2.037	226	0.90
NDUL	203	81	8.05	102	1,468	291	1.610	194	0.96
NDSH	245	119	10.1	155	2,261	502	1.970	226	0.92
NDSL	198	77	7.59	91	1,344	258	1.375	194	0.98

Note: S for side bonded; U for U-wrap; C for continuous; D for discontinuous; LD for low-density; HD for high-density.
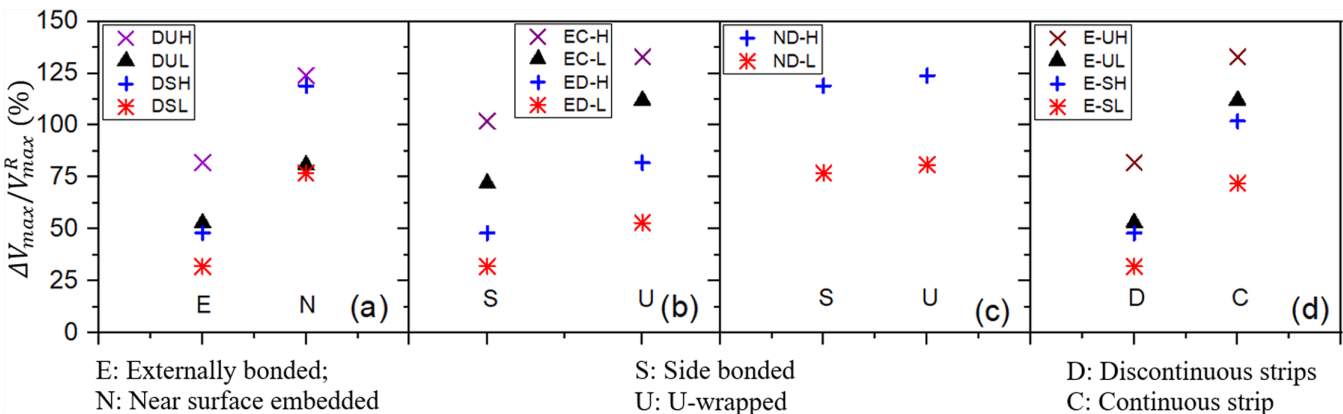

FIGURE 5 Effect the strengthening technique (a), strengthening scheme for EB-SRG (b) and NSE-SRG (c) strengthened beams, and strengthening amount (d) on the percentage increase in *Vmax*. EB, externally bonded; NSE, near − surface embedded; SRG, steel reinforced grout

and SRG-strengthened beam, respectively, then the percentage increase in the shear capacity ($\Delta V_{max}/V_{max}^R$) can be evaluated as listed in Table 2.

3.1 | Shear capacity

All the tested beams exhibited shear failure before flexural failure with the formation of diagonal cracks in the test span. The reference beam failed at a maximum shear load of 112 kN, as presented in Table 2, whereas all the strengthened beams failed at a higher shear load than that of the reference specimen; however, the percentage increase in V_{max} was influenced by the test parameters.

Figure 5a–d show the variation in the shear capacity increase with the test parameters for the strengthened beams. It can be observed from Figure 5a–d and Table 2 that the values of $\Delta V_{max}/V_{max}^R$ for the NSE-SRG strengthened beams varied from 77% to 124%, whereas it varied from 32% to 133% for the EB-SRG. As shown in Figure 5a, the NSE-SRG strengthened specimens showed a higher increase in V_{max} compared with the EB-SRG beams regardless of the fabric density and the SRG application method. For instance, Specimen NDSH, which was strengthened with NSE side bonded discontinuous SRG strips comprising high-density steel fabrics, failed at a shear load of 250 kN representing 119% increase in V_{max} relative to R, which is 71% higher than that of the

corresponding EB-SRG strengthened beams, namely Specimen EDSH. The average values of $\Delta V_{max}/V_{max}^R$ was 98% for the side bonded and 102% for the U-wrapped NSE-SRG strengthened beams. The corresponding average values for the EB-SRG strengthened beams were 40% for the side bonded SRG and 68% for the U-wrapped SRG. This result is possibly related to the failure modes of the beams. The NSE technique improved the strengthening performance of the SRG system by delaying and/or precluding premature SRG debonding. Therefore, premature debonding failure can be controlled in the NSE-SRG system, unlike in the EB-SRG where the beams experienced premature SRG debonding. Thus, the SRG strengthening system was more effective when applied as NSE compared with that of externally bonded SRG.

Figure 5b,c show the effect of the strengthening scheme on the shear strength gains of EB-SRG and NSE-SRG strengthened beams, respectively. For the EB-SRG system, the U-wrap SRG resulted in a higher $\Delta V_{max}/V_{max}^R$ value compared with that of the corresponding side bonded beam, as can be seen in Figure 5b. For instance, Specimens EDUL and EDUH, which were strengthened with discontinuous U-jacketed SRG, failed at shear loads of 171 kN and 204 kN corresponding to 53% and 82% increase in V_{max}, respectively. The corresponding side bonded SRG-strengthened beams, namely Specimens EDSL and EDSH, failed at lower shear loads of 147 kN and 166 kN representing $\Delta V_{max}/V_{max}^R$ values of 32% and 48%, respectively. On average, the U-jacketed EB-SRG showed 36% and 28% higher increase in V_{max} compared with those of the corresponding side bonded EB-SRG beams for continuous and discontinuous SRG strips, respectively. The strengthening scheme did not significantly influence the values of $\Delta V_{max}/V_{max}^R$ for the NSE-SRG strengthened beams, as shown in Figure 5c. The maximum shear load in Specimens NDUH and NDSH were 250 kN and 245 kN, respectively, which are nearly equal. Similarly, the difference in the shear capacity of Specimens NDUL (203 kN) and NDSL (198 kN) was not significant, as presented in Table 2. On average, the difference in the values of $\Delta V_{max}/V_{max}^R$ was only 4.46% for the beams strengthened with the side bonded and U-wrapped NSE-SRG system. Thus, for the NSE-SRG system, the effect of the wrapping scheme is negligible compared with that of the EB-SRG. This result can be explained using the failure modes of the beams. The use of U-wrap scheme in the EB-SRG allowed it to fail at a later stage compared with the side bonded EB-SRG. However, for the NSE-SRG, both the side bonded SRG and U-wrapped SRG strengthened beams exhibited similar type of failure.

Regarding the strengthening amount, the increase in the SRG reinforcement in continuous SRG configuration led to a higher increase in V_{max}, as shown in Figure 5d. The average values of $\Delta V_{max}/V_{max}^R$ were 105% and 54% for continuous and discontinuous EB-SRG strips, respectively. In addition, specimens strengthened with SRG made of high-density steel fabrics exhibited higher shear capacity compared with that of low-density fabrics, as shown in Figure 5d and Table 2. The axial rigidity of the SRG composite (K_{sf}) was used to perform a better comparison of the effect of different steel fabric densities and the amount of SRG reinforcement in the shear span (influenced by the strengthening configuration). The axial rigidity is defined as the product of the geometric reinforcement ratio of the steel fabrics in the SRG composite (ρ_{sf}) and its elastic modulus (E_{sf}), as given in Equation (1).

$$K_{sf} = \rho_{sf} E_{sf}. \tag{1}$$

The geometric reinforcement ratio of SRG is a function of the amount of the SRG reinforcement, which in turn is influenced by the strengthening configuration, as given below.

$$\rho_{sf} = F \frac{n_{sf}\, t_{sf}}{b_w}. \tag{2}$$

The reduction factor, F in Equation (2) indicates the proportion of the critical shear span (a) strengthened with the SRG system, as given in Equation (3) for discontinuous configuration, whereas F is unity for continuous configuration.

$$F = \frac{N_{srg}\, w_{srg}}{a}, \tag{3}$$

where w_{srg} and N_{srg} are the width and the number of SRG strips, respectively, b_w is the beam width, t_{sf} is the area of the steel fibers per unit width, as defined earlier, and n_{sf} is the number of steel fabric layers (2 in this study).

Figure 6a–c show the effect of the axial rigidity on the percentage increase in V_{max} for low- and high-density EB-SRG strengthened beams; Figure 6c shows the variation in the increase in V_{max} with K_{sf} for the NSE-SRG strengthened beams. As shown in these figures, an increase in K_{sf} results in an increase in $\Delta V_{max}/V_{max}^R$; however, the result shows a non-proportional relationship between $\Delta V_{max}/V_{max}^R$ and K_{sf}. An increase in the SRG amount in the continuous strip leads to an increase in the axial rigidity of SRG compared with the discontinuous strips, which in turn increases $\Delta V_{max}/V_{max}^R$, as shown in Figure 6a–c. An increase in the fabric density results in a higher axial rigidity, which in turn increases
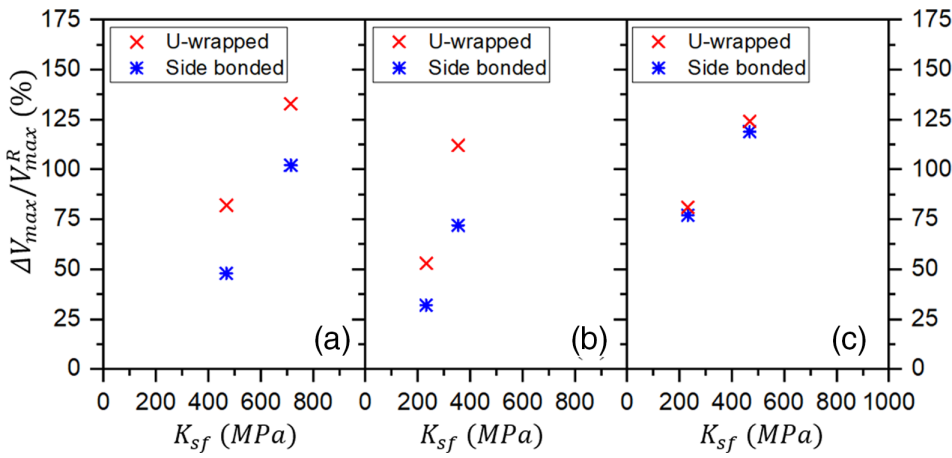
FIGURE 6 Effect of the axial rigidity on the percentage increase in *Vmax* for the specimens strengthened with (a) high-density EB-SRG, (b) low-density EB-SRG, and (c) NSE-SRG. EB, externally bonded; NSE, near-surface embedded; SRG, steel reinforced grout
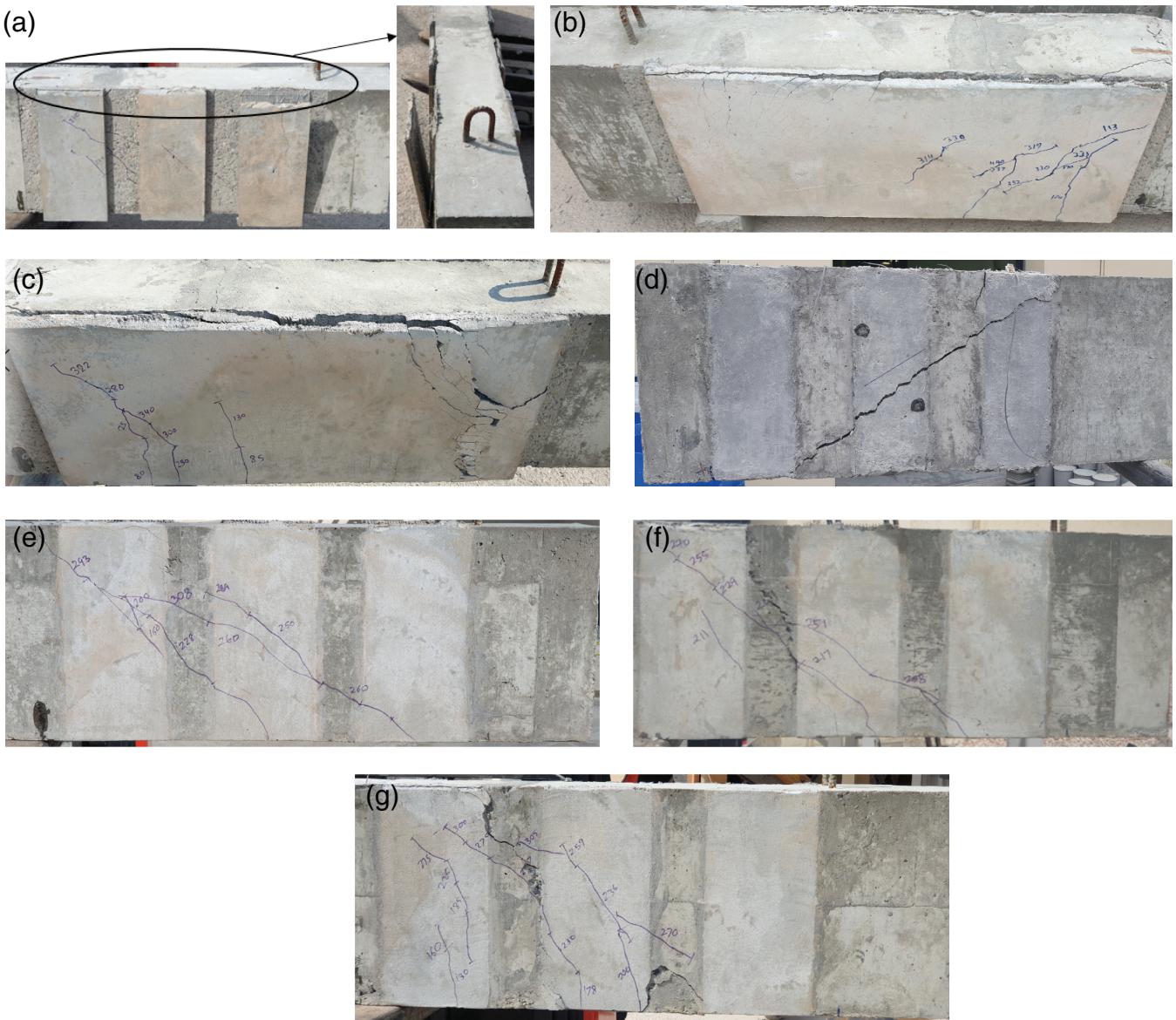
FIGURE 7 Crack pattern and failure modes

the shear contribution of the SRG composite; this result is consistent with those of the FRCM-strengthened beams.[49]

3.2 | Observed failure modes

Figure 7a–g show the representative failure patterns of the strengthened beams. It should be noted that the values of the load marked on the beams in these figures are the applied load values and not the shear load. The failure mode of the reference specimen is a typical shear failure pattern with the formation of diagonal shear crack. The failure in the strengthened beams depends on the test parameters, namely the strengthening technique and the type of the SRG application method (for EB-SRG), as shown in Figure 7a–g. This is discussed below.

i. SRG debonding: the common failure mode observed in the EB-SRG beams was debonding of the SRG laminate. Debonding occurred at the fiber/matrix interface in the specimens strengthened with high-density SRG fabrics, as shown in Figure 7a for Specimen EDUH and Figure 7b for Specimen ECUH. However, the failure of the beams strengthened with SRG comprising low-density steel fabrics involved debonding of SRG with cover concrete, as can be seen in Figure 7c for Specimen ECUL. In both continuous and discontinuous EB-SRG, the use of a U-wrap strengthening scheme delayed the occurrence of SRG debonding failure by allowing the beam to fail at a later stage compared with the side bonded EB-SRG.

ii. Complete/partial rupture of steel fabrics: for the NSE-SRG beams, failure was followed by fabric rupture without any sign of SRG debonding, as can be seen in Figure 7d–f for Specimens NDUH, NDUL, and NDSL, except for Specimen NDSH. Failure in Specimen NDSH involved partial debonding of the first two SRG strips, as shown in Figure 7g. The application of SRG composite using the NSE technique provided inherent anchorage for the SRG laminate and hence mitigated or delayed the premature debonding failure observed in the EB-SRG strengthened beams. Consequently, the NSE-SRG resulted in better utilization of the composite.

3.3 | Deformational characteristics

The shear load versus displacement under the load for the NSE-SRG and EB-SRG strengthened beams is shown
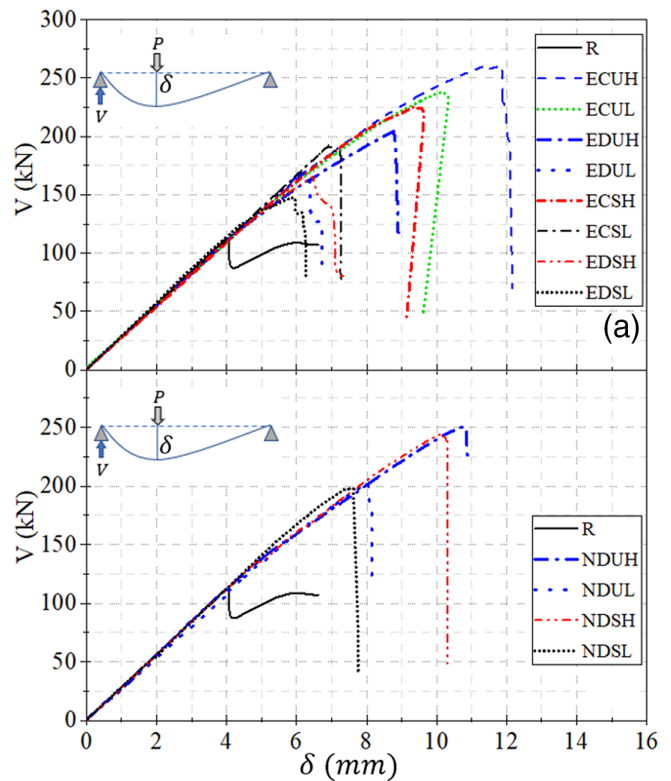

FIGURE 8 Shear load versus deflection under the loading point for (a) EB-SRG and (b) NSE-SRG strengthened beams. EB, externally bonded; NSE, near-surface embedded; SRG, steel reinforced grout

in Figure 8a,b, respectively. The deflection was linear until the peak shear load in all the tested beams. The maximum deflection (δ_{max}) corresponding to V_{max} in all the strengthened beams was larger than that of the reference (3.97 mm). The values of δ_{max} were 11.40 mm and 10.8 mm for the EB-SRG and NSE-SRG strengthened beams, respectively. The NSE-SRG strengthened beams had higher values of δ_{max} compared with the EB-SRG beams, as presented in Table 2. The strengthened beams showed considerably higher deflection relative to the reference beam, as can be seen in Figure 8a,b and Table 2. This result confirms that the SRG strengthening can substantially increase the deformation capacity of the strengthened beams. The specimens strengthened with NSE-SRG showed a higher increase in δ_{max} compared with the EB-SRG counterparts, as given in Table 2. On average, the increase in δ_{max} was 130% for EB-SRG strengthened beams and 72% for the NSE-SRG strengthened beams.

Figure 9a,b show the relationship between the shear load and the strains developed in the flexural tensile bars for beams strengthened with continuous and discontinuous SRG strips. It can be observed from the figures that shear failure in all the beams occurred prior to flexural yielding, except for Specimen NDUH that failed after the

yielding of flexural bars. Furthermore, the strains developed in the concrete at V_{max} were below the concrete crushing strain of 0.35%, as presented in Table 2. In addition, NSE-SRG increased the strains developed in the tensile reinforcement compared with the EB-SRG beams.

The efficacy of the strengthening system can also be studied in terms of the energy absorption (ψ), which is defined as the area under the applied load (P) versus the deflection under the load curve up to the maximum load.
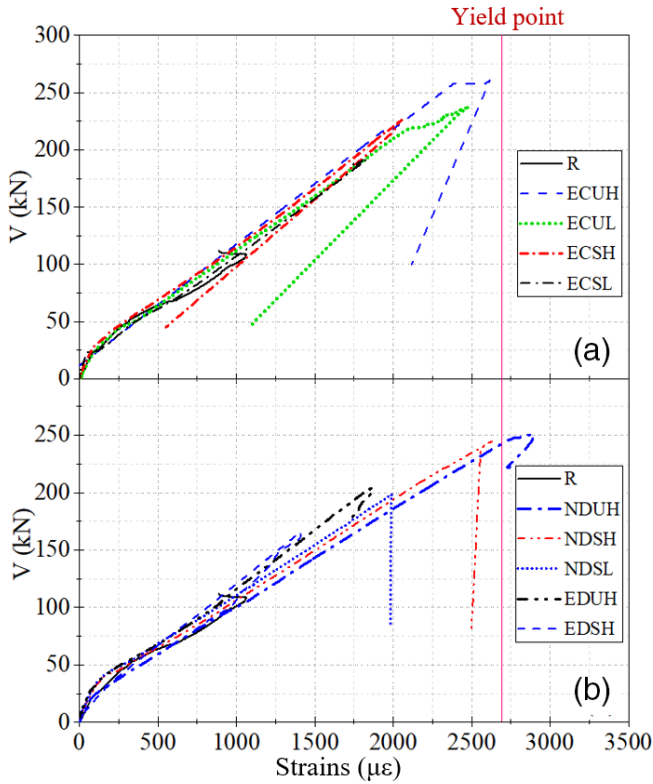

FIGURE 9 Shear load versus tensile strain developed in the flexural bars for beams strengthened with (a) continuous SRG strip and (b) discontinuous SRG strips. SRG, steel reinforced grout

The energy absorption for the reference beam is 375.6 kN·mm, as presented in Table 2. The strengthened beams exhibited substantially higher values of ψ compared with the reference beam. The increase in ψ ($\Delta\psi$) ranged from 121% to 649% for the EB-SRG strengthened beams and 258% to 566% for the NSE-SRG strengthened beams. Figure 10a–d show variations in the increase in ψ with the test parameters. The value of $\Delta\psi$ is higher in the NSE-SRG strengthened beams than in the EB-SRG beams, as shown in Figure 10a. Hence, the use of the NSE technique resulted in a higher strengthening efficacy of the SRG. Moreover, the U-wrap scheme in the EB-SRG significantly increased the strengthening capability of the SRG system, except for Specimen EDUL where the difference in $\Delta\psi$ was only 23%, as shown in Figure 10b. However, the difference in the increase in ψ was insignificant in the NSE-SRG beams with side-bonded or U-wrap scheme, as shown in Figure 10c and Table 2. It can be observed from Figure 10d that increasing the strengthening amount in continuous EB-SRG increases the gain ψ. Furthermore, as presented in Table 2, an increase in the density of the SRG fabrics increased its strengthening efficacy.

4 | ANALYTICAL FORMULATION

A model based on the simplified compression field theory (SCFT) was formulated to predict the shear capacity of both the NSE-SRG and the EB-SRG strengthened beams. Consider the NSE-SRG strengthened RC beam in Figure 11a with no internal shear reinforcement within the critical shear span. From Figure 11, the clamping stress (f_y) is given in terms of the concrete diagonal tensile stress (f_1) and diagonal tensile stress (f_2), and inclination of diagonal compressive stress (θ):
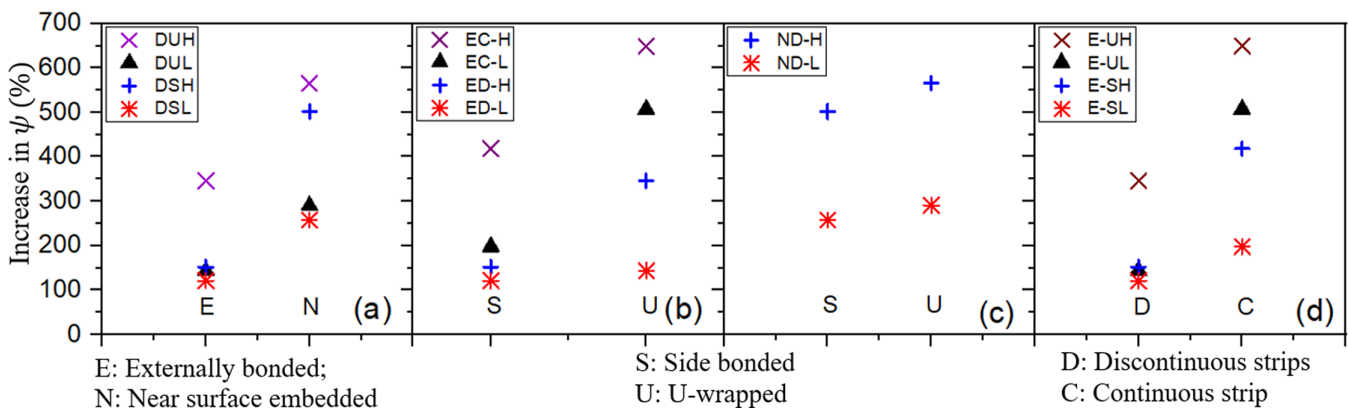
FIGURE 10 Effect the strengthening technique (a), strengthening scheme for EB-SRG (b) and NSE-SRG (c) strengthened beams, and strengthening amount (d) on the percentage increase in the energy absorption of the strengthened beams. EB, externally bonded; NSE, near-surface embedded; SRG, steel reinforced grout
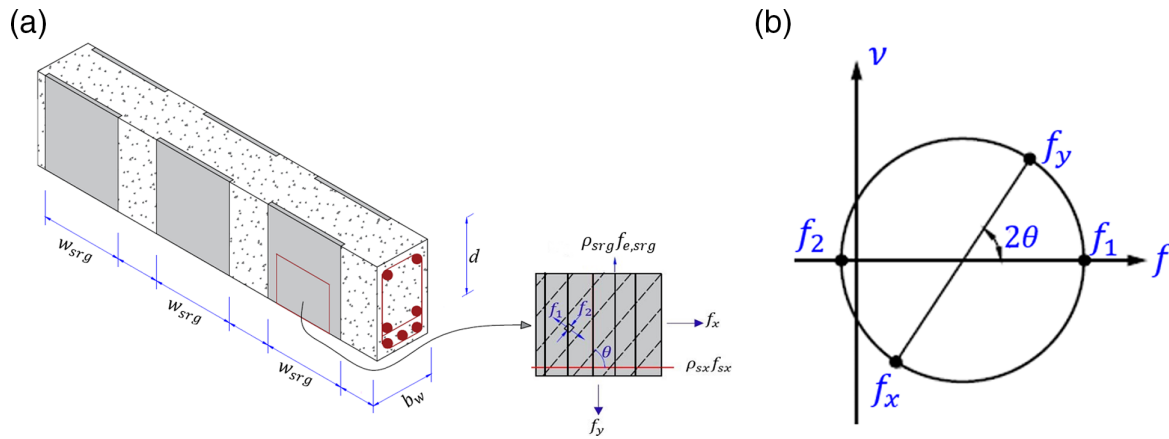
FIGURE 11 SRG-strengthened beam shear model based on the MCFT.[50] SRG, steel reinforced grout

$$f_y = \rho_{srg}f_{e,srg} + f_1 + (f_1 cos^2\theta - f_2 sin^2\theta). \quad (4)$$

From Figure 11b, the ultimate shear stress (v) can be given by:

$$v = \frac{f_1 + f_2}{tan\theta + cot\theta}. \quad (5)$$

The clamping stress in Equation (4) is negligible.[51] Therefore, combining Equation (4) and Equation (5), the ultimate shear stress is given by:

$$v = f_1 cot\theta + \rho_{srg}f_{e,srg}cot\theta. \quad (6)$$

The value of f_1 is given as follows in terms of the compressive strength of concrete (f'_c) and tensile stress factor (β)[51]:

$$v = \beta\sqrt{f'_c}. \quad (7)$$

The value of β is given in terms of the flexural strain (ϵ_x) and crack spacing (S_{xe})[51]:

$$\beta = \frac{0.4}{1 + 1500\,\epsilon_x}\frac{1300}{1000 + S_{xe}}. \quad (8)$$

Moreover, the inclination θ of the compressive stress is given by[51]:

$$\theta = (29 + 7000\,\epsilon_x) \times \left(0.88 + \frac{S_{xe}}{2500}\right) \le 75°. \quad (9)$$

For RC beams without internal shear reinforcement, the value of S_{xe} is given by[51]:

$$S_{xe} = \frac{35S_x}{a_g + 16} \ge 0.85S_x. \quad (10)$$

where S_x is the vertical distance between the top and bottom bars and a_g is the maximum aggregate size.

The equilibrium of stresses is considered in order to determine the strain ϵ_x. The externally applied stress in the x-direction can be given as:

$$f_x = \rho_{sx}f_{sx} + f_1 sin^2\theta - f_2 cos^2\theta. \quad (11)$$

where ρ_{sx} is the reinforcement ratio of the flexural tensile bars. There is no externally applied stress in the x-direction, $f_x = 0$. Therefore, the stress in the flexural reinforcement can be given by:

$$f_{sx} = (f_2 cos^2\theta - f_1 sin^2\theta)/\rho_{sx}. \quad (12)$$

Thus, the value of ϵ_x is given by:

$$\epsilon_x = \frac{(f_2 cos^2\theta - f_1 sin^2\theta)}{(\rho_{sx}E_{sx})}, \quad (13)$$

where E_{sx} is the elastic modulus of the longitudinal tensile reinforcement bars. Combining Equation (6), Equation (7), and Equation (13), the value of ϵ_x can be given by:

$$\epsilon_x = \frac{v cot\theta - \beta\sqrt{f'_c}\,tan\theta}{E_s\rho_{sx}}. \quad (14)$$

Therefore, the shear strength is given as:

$$v = \beta\sqrt{f'_c} + \rho_{srg}f_{e,srg}cot\theta. \quad (15)$$

The first part of Equation (15) represents the contribution of concrete to the shear strength and the second

part represents the shear strength contribution of SRG strengthening.

To determine the effective stress developed in SRG, we adopted the method proposed by Chen and Teng,[52] which was originally developed for RC beams strengthened with FRP. This model has shown to provide a reasonable prediction for the effective stress developed in FRCM.[53] Accordingly, the value of $f_{e,srg}$ is given as follows:

$$f_{e,srg} = D_{srg} f_{u,srg}. \tag{16}$$

where D_{srg} is the stress distribution factor and $f_{max,srg}$ is the maximum stress in SRG given by Equation (17), which should not exceed the tensile strength of the SRG steel fibers ($f_{t,sf}$) given in Table 1:

$$f_{max,srg} = 0.427 \beta_w \beta_L \sqrt{\frac{E_{sf} \sqrt{f'_c}}{t_{sf}}} \le f_{t,sf}. \ (MPa \cdot mm). \tag{17}$$

For the NSE-SRG strengthened beam without SRG debonding, the value of $f_{max,srg}$ is given as:

$$f_{max,srg} = 0.724 \beta_w \beta_L \sqrt{\frac{E_{sf} \sqrt{f'_c}}{t_{sf}}} \le f_{t,sf} \ (MPa \cdot mm). \tag{18}$$

where $\beta_w = 1/\sqrt{2}$ for the continuous configuration and β_L is a factor that indicates the bond length, and is given by:

$$\beta_L = \begin{cases} sin\pi\lambda/2, & \lambda < 1 \\ 1, & \lambda \ge 1 \end{cases}. \tag{19}$$

The stress distribution factor is determined based on the normalized maximum bond length parameter ($\lambda = L_{max}/L_e$), as given in Equation (20).

$$D_{srg} = \begin{cases} 1 - \dfrac{\pi-2}{\pi\lambda}, & \lambda > 1 \\ \dfrac{2}{\pi\lambda} \dfrac{1-cos\pi\lambda/2}{sin\pi\lambda/2}, & \lambda \le 1 \end{cases}. \tag{20}$$

where L_{max} is the available bond length, $L_{max} = d_{srg}$ for the U-wrapped SRG and $L_{max} = d_{srg}$ for the side-bonded SRG, whereas L_e is the effective bond length, which is given as:

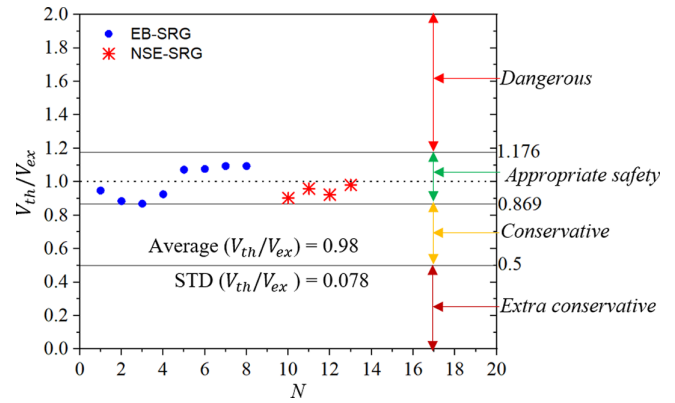$$L_e = \sqrt{\frac{E_{srg} t_{srg}}{\sqrt{f'_c}}}. \tag{21}$$

FIGURE 12 Prediction capability of the adopted formulations

TABLE 3 Modified demerits points classification criteria[54]

V_{th}/V_{ex}	Classification	Penalty
> 2	Extra dangerous	10
(1.176–2)	Dangerous	5
(0.869–1.176)	Appropriate safety	0
(0.5–0.869)	Conservative	1
≤ 0.5	Extra conservative	2

where $d_{srg} = 0.9d$ is the effective depth of the SRG strengthening.

The theoretically predicted shear capacity (V_{th}) and the V_{th}/V_{ex} ratio are given in Table 2. The proposed model gives accurate predictions for both EB-SRG and NSE-SRG strengthened beams with an average V_{th}/V_{ex} of 0.98 and a standard deviation of 0.078. The modified demerit points classification was also used to further evaluate the capability of the model, as shown in Figure 12. In this method, a penalty is assigned to each value of V_{th}/V_{ex} to evaluate the model in terms of accuracy, economic, and safety aspects as listed in Table 3.[54] As can be seen in Figure 12, the prediction results of all the beams are within an appropriate safety region. Therefore, the model resulted in safe and accurate predictions of the shear capacity of both the NSE-SRG and EB-SRG strengthened beams tested in this study.

5 | CONCLUSIONS

This paper reported the results of experiments on the shear performance of RC beams strengthened in shear using different techniques for an SRG system. The experiment involved 13 rectangular RC beams with dimensions of 180 mm × 400 mm × 2,550 mm subjected to monotonically increasing three-point loading. Two different techniques were used, namely, the NSE and

the conventional externally bonded technique. Moreover, the effects of the fabric density, strengthening scheme (side-bonded versus U-wrapped SRG), and strengthening amount in a continuous or discontinuous configuration on the strengthening performance of the SRG system were examined. The results of the study support the following conclusions:

1. The SRG system substantially increased the shear capacity of the beams. The increase in the shear capacity of the strengthened beams relative to the reference beam ranged from 32 to 132%.

2. The strength properties of the SRG steel fiber can be better utilized by employing the NSE technique. The failure mode of the strengthened beams can be changed from SRG laminate debonding failure to SRG fabric rupture failure using the NSE technique. The failure of the NSE-SRG strengthened beams was mainly characterized by fabric rupture, unlike the EB-SRG beams where failure was attributed to premature SRG debonding. Thus, the former represents a better utilization of the SRG system. The increase in V_{max} relative to the reference beam ranged from 81% to 124% for the NSE-SRG strengthened beams and 32% to 82% for the corresponding discontinuous EB-SRG strengthened beams.

3. The average $\Delta V_{max}/V_{max}^R$ values for the EB-SRG with a U-wrapped SRG are 36% and 28% higher compared with those of the side bonded counterpart for the continuous and discontinuous SRG strips, respectively. However, the difference in the average $\Delta V_{max}/V_{max}^R$ was less than 4.46% for the NSE-SRG. Thus, unlike in the EB technique, the wrapping scheme in the NSE technique has minimal effect on both the shear strength and the failure modes of the strengthened beams.

4. The axial rigidity of the SRG composite was used to ensure a better comparison between the different strengthening configurations and the steel fabric densities. The continuous SRG configuration was more effective than the discontinuous strips, and the shear capacity of the beam increased with an increase in K_{sf}.

5. Finally, an analytical procedure was proposed to predict the shear strength of RC beams strengthened with both the NSE-SRG and EB-SRG taking the type of the strengthening technique into consideration.

Further research should focus on other factors affecting the performance of the SRG system such as the presence of end anchorage.

DATA AVAILABILITY STATEMENT

Data available on request from the authors.

ORCID

Usama Ebead https://orcid.org/0000-0001-9121-8387

REFERENCES

1. Tetta ZC, Bournas D. TRM vs FRP jacketing in shear strengthening of concrete members subjected to high temperatures. Compos Part B: Eng. 2016;106:190–205. https://doi.org/10.1016/j.compositesb.2016.09.026.

2. Koutas L, Tetta ZC, Bournas D, et al. Strengthening of concrete structures with textile reinforced mortars: State-of-the-art review. J Compos Construction. 2019;23:03118001. https://doi.org/10.1061/(ASCE)CC.1943-5614.0000882.

3. Babaeidarabad S, Loreto G, Nanni A. Flexural strengthening of RC beams with an externally bonded fabric-reinforced cementitious matrix. J Compos Construction. 2014;18:1–12. https://doi.org/10.1061/(ASCE)CC.1943-5614.0000473.

4. Oller E, Pujol M, Marí A. Contribution of externally bonded FRP shear reinforcement to the shear strength of RC beams. Compos Part B: Eng. 2019;164:235–248. https://doi.org/10.1016/j.compositesb.2018.11.065.

5. Pellegrino C, Modena C. Fiber reinforced polymer shear strengthening of reinforced concrete beams with transverse steel reinforcement. J Compos Construction. 2002;6:104–111. https://doi.org/10.1061/(ASCE)1090-0268(2002)6:2(104).

6. Tzoura E, Triantafillou TC. Shear strengthening of reinforced concrete T-beams under cyclic loading with TRM or FRP jackets. Mater Struct. 2016;49:17–28. https://doi.org/10.1617/s11527-014-0470-9.

7. Ozden S, Atalay HM, Akpinar E, Erdogan H, Vulaş YZ. Shear strengthening of reinforced concrete T-beams with fully or partially bonded fibre-reinforced polymer composites. Struct Concrete. 2014;15:229–239. https://doi.org/10.1002/suco.201300031.

8. Zhang D, Shi H, Ueda T, Jin W. Effect of U-shaped anchorages on concrete cover separation in carbon fiber-reinforced polymer-strengthened beams with notches at the sheet end. Struct Concrete. 2020;1–19. https://doi.org/10.1002/suco.201900388.

9. Dias SJE, Barros JAO, Janwaen W. Behavior of RC beams flexurally strengthened with NSM CFRP laminates. Compos

Struct. 2018;201:363–376. https://doi.org/10.1016/j.compstruct.2018.05.126.

10. Bilotta A, Ceroni F, Nigro E, Pecce M. Efficiency of CFRP NSM strips and EBR plates for flexural strengthening of RC beams and loading pattern influence. Compos Struct. 2015;124:163–175. https://doi.org/10.1016/j.compstruct.2014.12.046.

11. Dias SJE, Barros JAO. NSM shear strengthening technique with CFRP laminates applied in high T cross section RC beams. Compos Part B: Eng. 2017;114:256–267. https://doi.org/10.1016/j.compositesb.2017.01.028.

12. Dias SJE, Barros JAO. Performance of reinforced concrete T-beams strengthened in shear with NSM CFRP laminates. Eng Struct. 2010;32:373–384. https://doi.org/10.1016/j.engstruct.2009.10.001.

13. Zhang SS, Yu T, Chen GM. Reinforced concrete beams strengthened in flexure with near-surface mounted (NSM) CFRP strips: Current status and research needs. Compos Part B: Eng. 2017;131:30–42. https://doi.org/10.1016/j.compositesb.2017.07.072.

14. Aljazaeri ZR, Myers JJ. Flexure performance of RC one-way slabs strengthened with composite materials. J Mater Civil Eng. 2018;30:04018120. https://doi.org/10.1061/(asce)mt.1943-5533.0002299.

15. Harajli M, ElKhatib H, San-Jose JT. Static and cyclic out-of-plane response of masonry walls strengthened using textile-mortar system. J Mater Civil Eng. 2010;22:1171–1180. https://doi.org/10.1061/(ASCE)MT.1943-5533.0000128.

16. D'Antino T, Focacci F, Sneed LH, et al. Shear strength model for RC beams with U-wrapped FRCM composites. J Compos Construction. 2020;24:04019057. https://doi.org/10.1061/(ASCE)CC.1943-5614.0000986.

17. Akbari Hadad H, Erickson B, Nanni A. Flexural analysis and design of FRCM-strengthened RC beams. Construction Building Mater. 2020;244:118371. https://doi.org/10.1016/j.conbuildmat.2020.118371.

18. Younis A, Ebead U, Shrestha K. Tensile characterization of multi-ply fabric-reinforced cementitious matrix strengthening systems. Struct Concrete. 2019;21:713–723. https://doi.org/10.1002/suco.201900076.

19. Wakjira T, Ebead U. FRCM/internal transverse shear reinforcement interaction in shear strengthened RC beams. Compos Struct. 2018;201:326–339. https://doi.org/10.1016/j.compstruct.2018.06.034.

20. Wakjira T, Ebead U. Hybrid NSE/EB technique for shear strengthening of reinforced concrete beams using FRCM: Experimental study. Construction Building Mater. 2018;164:164–177. https://doi.org/10.1016/j.conbuildmat.2017.12.224.

21. El-Sherif HE, Wakjira TG, Ebead U. Flexural strengthening of reinforced concrete beams using hybrid near-surface embedded/externally bonded fabric-reinforced cementitious matrix. Construction Build Mater. 2020;238:117748. https://doi.org/10.1016/j.conbuildmat.2019.117748.

22. Ekenel M, Caso FD, Nanni A. Acceptance criteria for concrete and masonry strengthening using fabric- reinforced cementitious matrix (FRCM) and steel reinforced grout (SRG) composites. ACI Special Publication. 2018;324-04:4.1–4.6.

23. De Santis S, De Felice G, Napoli A, et al. Strengthening of structures with steel reinforced polymers: A state-of-the-art review. Compos Part B: Eng. 2016;104:87–110. https://doi.org/10.1016/j.compositesb.2016.08.025.

24. Huang X, Birman V, Nanni A, Tunis G. Properties and potential for application of steel reinforced polymer and steel reinforced grout composites. Compos Part B: Eng. 2005;36:73–82. https://doi.org/10.1016/S1359-8368(03)00080-5.

25. De Santis S, De Felice G. Steel reinforced grout systems for the strengthening of masonry structures. Compos Struct. 2015;134:533–548. https://doi.org/10.1016/j.compstruct.2015.08.094.

26. De Santis S, Roscini F, de Felice G. Full-scale tests on masonry vaults strengthened with steel reinforced grout. Compos Part B: Eng. 2018;141:20–36. https://doi.org/10.1016/j.compositesb.2017.12.023.

27. Sneed LH, Baietti G, Fraioli G, Carloni C. Compressive behavior of brick masonry columns confined with steel-reinforced grout jackets. J Compos Construction. 2019;23:04019037. https://doi.org/10.1061/(ASCE)CC.1943-5614.0000963.

28. Mazzuca S, Hadad HA, Ombres L, Nanni A. Mechanical characterization of steel-reinforced grout for strengthening of existing masonry and concrete structures. J Mater Civil Eng. 2019;31:04019037. https://doi.org/10.1061/(ASCE)MT.1943-5533.0002669.

29. Barton B, Wobbe E, Dharani LR, et al. Characterization of reinforced concrete beams strengthened by steel reinforced polymer and grout (SRP and SRG) composites. Materials sci Eng: A. 2005;412:129–136. https://doi.org/10.1016/j.msea.2005.08.151.

30. Napoli A, Realfonzo R. Reinforced concrete beams strengthened with SRP/SRG systems: Experimental investigation. Construction Build Mater. 2015;93:654–677. https://doi.org/10.1016/j.conbuildmat.2015.06.027.

31. Prota A, Tan KY, Nanni A, et al. Performance of shallow reinforced concrete beams with externally bonded steel-reinforced polymer. ACI Struct J. 2006;103:163–170. https://doi.org/10.14359/15173

32. Balsamo A, Nardone F, Iovinella I, Ceroni F, Pecce M. Flexural strengthening of concrete beams with EB-FRP, SRP and SRCM: Experimental investigation. Compos Part B: Eng. 2013;46:91–101. https://doi.org/10.1016/j.compositesb.2012.10.014.

33. Ombres L, Verre S. Flexural strengthening of RC beams with steel-reinforced grout: Experimental and numerical investigation. J Compos Construction. 2019;23:04019035. https://doi.org/10.1061/(ASCE)CC.1943-5614.0000960.

34. Thermou GE, Hajirasouliha I. Compressive behaviour of concrete columns confined with steel-reinforced grout jackets. Compos Part B: Eng. 2018;138:222–231. https://doi.org/10.1016/j.compositesb.2017.11.041.

35. Wakjira TG, Nehdi ML, Ebead U. Fractional factorial design model for seismic performance of RC bridge piers retrofitted with steel-reinforced polymer composites. Eng Struct. 2020;221:111100. https://doi.org/10.1016/j.engstruct.2020.111100.

36. Thermou GE, Katakalos K, Manos G. Influence of the cross section shape on the behaviour of SRG-confined prismatic concrete specimens. Mater Struc. 2016;49:869–887. https://doi.org/10.1617/s11527-015-0545-2.

37. Santandrea M, Focacci F, Mazzotti C, et al. Determination of the interfacial cohesive material law for SRG composites bonded to a masonry substrate. Eng Failure Analysis. 2020;111:104322. https://doi.org/10.1016/j.engfailanal.2019.104322.

38. Lopez A, Galati N, Alkhrdaji T, Nanni A. Strengthening of a reinforced concrete bridge with externally bonded steel reinforced polymer (SRP). Compos Part B: Eng. 2007;38: 429–436. https://doi.org/10.1016/j.compositesb.2006.09.003.

39. Triantafillou T, Papanicolaou C. Shear strengthening of reinforced concrete members with textile reinforced mortar (TRM) jackets. Mater Struct. 2006;39:93–103. https://doi.org/10.1617/s11527-005-9034-3

40. Sneed L, Verre S, Carloni C, et al. Flexural behavior of RC beams strengthened with steel-FRCM composite. Eng Struct. 2016;127:686–699. https://doi.org/10.1016/j.engstruct.2016.09.006.

41. Wakjira TG, Ebead U. Experimental and analytical study on strengthening of reinforced concrete T-beams in shear using steel reinforced grout (SRG). Compos Part B: Eng. 2019;177: 107368. https://doi.org/10.1016/j.compositesb.2019.107368.

42. Thermou GE, Papanikolaou VK, Lioupis C, Hajirasouliha I. Steel-reinforced grout (SRG) strengthening of shear-critical RC beams. Construction Build Mater. 2019;216:68–83. https://doi.org/10.1016/j.conbuildmat.2019.04.259.

43. Wakjira TG, Ebead U. Shear span-to-depth ratio effect on steel reinforced grout strengthened reinforced concrete beams. Eng Struct. 2020;216:110737. https://doi.org/10.1016/j.engstruct.2020.110737.

44. Wakjira T, Ebead U. Internal transverse reinforcement configuration effect of EB/NSE-FRCM shear strengthening of RC deep beams. Compos Part B: Eng. 2019;166:758–772. https://doi.org/10.1016/j.compositesb.2019.03.004.

45. Lorenzis LD, Teng JG. Near-surface mounted FRP reinforcement: An emerging technique for strengthening structures. Compos Part B: Eng. 2007;38:119–143. https://doi.org/10.1016/j.compositesb.2006.08.003.

46. D'Antino T, Pisani MA. Evaluation of the effectiveness of current guidelines in determining the strength of RC beams retrofitted by means of NSM reinforcement. Compos Struct. 2017;167:166–177. https://doi.org/10.1016/j.compstruct.2017.01.070.

47. Ibrahim M, Wakjira T, Ebead U. Shear strengthening of reinforced concrete deep beams using near-surface mounted hybrid carbon/glass fibre reinforced polymer strips. Eng Struct. 2020;210:110412. https://doi.org/10.1016/j.engstruct.2020.110412.

48. Kerakoll S.P.A, Accessed, December 25, http://www.kerakoll.com 2018.

49. Gonzalez-Libreros JH, Sneed LH, D'Antino T, et al. Behavior of RC beams strengthened in shear with FRP and FRCM composites. Eng Struct. 2017;150:830–842. https://doi.org/10.1016/j.engstruct.2017.07.084.

50. Vecchio FJ, Collins MP. The modified compression-field theory for reinforced concrete elements subjected to shear. ACI J Proc. 1986;83:219–231. https://doi.org/10.14359/10416.

51. Bentz EC, Vecchio FJ, Collins MP. Simplified compression field theory for calculating shear strength of reinforced concrete elements. ACI Struct J. 2006;103:614–624. https://doi.org/10.14359/16438.

52. Chen JF, Teng JG. Shear capacity of fiber-reinforced polymer-strengthened reinforced concrete beams: Fiber reinforced polymer rupture. J Structural Eng. 2003;129:615–625. https://doi.org/10.1061/(ASCE)0733-9445(2003)129:5(615).

53. Tetta ZC, Triantafillou T, Bournas D. On the design of shear-strengthened RC members through the use of textile reinforced mortar overlays. Compos Part B: Eng. 2018;147:178–196. https://doi.org/10.1016/j.compositesb.2018.04.008.

54. Neto BNM, Barros JAO, Melo GSSA. Model to simulate the contribution of fiber reinforcement for the punching resistance of RC slabs. J Mater Civil Eng. 2014;26:04014020. https://doi.org/10.1061/(ASCE)MT.1943-5533.

AUTHOR BIOGRAPHIES

Tadesse G. Wakjira, Department of Civil and Architectural Engineering, Qatar University, P.O. Box 2713, Doha, Qatar.

Usama Ebead, ASCE member, Professor of Structural Engineering, Department of Civil and Architectural Engineering, Qatar University, P. O. Box 2713, Doha, Qatar.